

# Meissner effect in superconducting microtraps

D. Cano,<sup>1</sup> B. Kasch,<sup>1</sup> H. Hattermann,<sup>1</sup> R. Kleiner,<sup>1</sup> C. Zimmermann,<sup>1</sup> D. Koelle,<sup>1</sup> and J. Fortágh<sup>1</sup>

<sup>1</sup>*Physikalisches Institut, Eberhard-Karls-Universität Tübingen,  
CQ Center for Collective Quantum Phenomena and their Applications,  
Auf der Morgenstelle 14, D-72076 Tübingen, Germany*

We report on the realization and characterization of a magnetic microtrap for ultra cold atoms near a straight superconducting Nb wire with circular cross section. The trapped atoms are used to probe the magnetic field outside the superconducting wire. The Meissner effect shortens the distance between the trap and the wire, reduces the radial magnetic-field gradients and lowers the trap depth. Measurements of the trap position reveal a complete exclusion of the magnetic field from the superconducting wire for temperatures lower than 6K. As the temperature is further increased, the magnetic field partially penetrates the superconducting wire; hence the microtrap position is shifted towards the position expected for a normal-conducting wire.

PACS numbers:

Microfabricated magnetic traps for cold atoms provide an intriguing physical scenario in which solid-state and atomic physics converge. Coherent control over the internal and external states of atomic quantum gases has already been achieved by means of magnetic potentials near microfabricated surfaces [1]. These advances led also to a number of fundamental studies of atom-surface interactions such as the spin decoherence of atoms near dielectric bodies [2, 3, 4, 5, 6] and the Casimir-Polder force between atoms and surfaces [7]. Superconductors are expected to play an essential role in this emerging field of research because they can provide an extremely low noise environment for trapped atoms [8]. Increased atomic coherence times at very short distances from superconducting surfaces will allow the manipulation of atomic wave functions even on the submicron scale. Also, it is likely that superconducting microstructures will have important applications which combine coherent atomic clouds with superconducting devices to form novel hybrid quantum systems. They include atomic hyperfine transitions coupled to local microwave sources made from Josephson junctions, or even quantum computation with single dipolar molecules [9] or Rydberg atoms that are coherently coupled by superconducting electrodes [10].

Recent experiments demonstrated the feasibility of superconducting microtraps [11] and the trapping of atoms nearby a persistent current loop [12]. The impact of the Meissner effect on the microtrap parameters has been assessed so far only theoretically [13]. The experimental observation of this fundamental property of superconductors requires short enough distances between the atoms and the superconducting surface. Understanding how the Meissner effect distorts magnetic potentials is a prerequisite for a new experimental regime in which the advantages of superconducting microstructures can be fully exploited.

In this letter we report on the realization of a magnetic microtrap for ultracold <sup>87</sup>Rb atoms near a superconducting niobium wire with circular cross section. By monitoring the position of the atom cloud, we observe the Meissner effect to influence the magnetic trap. Total

field exclusion from the Nb wire is observed for temperatures below 6 K. As the temperature of the Nb wire is increased the magnetic field gradually penetrates into the wire. Analytical expressions for describing the magnetic trap are deduced by approximating the superconducting wire to a perfectly diamagnetic cylinder.

The experimental system integrates the techniques for producing ultra cold atomic quantum gases with the techniques for cooling solid bodies to cryogenic temperatures. A standard, room-temperature trap setup for cooling atoms [1] and a Helium flow cryostat (ST-400 Janis) for operating superconducting microstructures are installed next to each other in a single vacuum chamber (Fig. 1). The vacuum chamber is evacuated to  $10^{-11}$  mbar by an ion pump and a titanium-sublimation pump. The transport of atoms from the room-temperature trap setup to the cryogenically cooled superconducting microstructure is accomplished by means of optical tweezers [14]. Such an arrangement is appropriate for trapping ultra cold atoms in superconducting microstructures which have to be thermally isolated from the environment and surrounded by a radiation shield.

The central piece of the experiment is a superconducting niobium (Nb) wire with circular cross section of diameter  $125\ \mu\text{m}$ , as shown in Fig. 2. The Nb wire is mechanically clamped between two gold-plated copper plates which are firmly attached to the Helium cryostat. This ensures mechanical stability and good thermal contact between the wire and the cryostat. The Nb wire is parallel to the  $z$ -axis. The microtrap is realized by applying an electric current  $I_{Nb}$  to the Nb wire and a homogeneous bias field  $\mathbf{B}_B$  along the  $x$ -direction [1]. Thus paramagnetic atoms can be radially confined around a line parallel to the Nb wire, where  $\mathbf{B}_B$  cancels the circular magnetic field of  $I_{Nb}$ . The microtrap is closed in the longitudinal direction by the magnetic field of two offset wires driven with equal currents  $I_0$  along the  $x$ -direction. The offset wires are separated by 3mm. Since the Nb wire is electrically not isolated from the Cu piece, the applied current  $I_{Nb}$  will entirely flow along the Nb wire only if this has no electrical resistance. Therefore, no microtrap

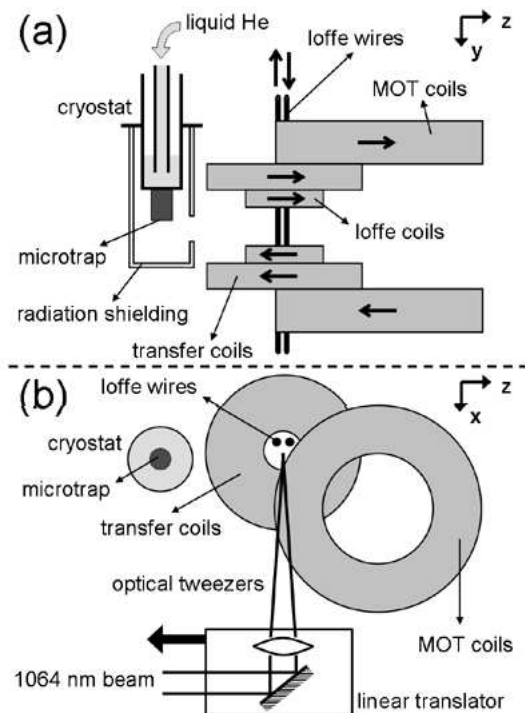


FIG. 1: Front view (a) and top view (b) of the experimental system combining a standard room-temperature trap setup (to the right) and a superconducting microtrap on a Helium flow cryostat (to the left). Atoms are initially prepared in MOT and magnetic trap, and subsequently transported to the superconducting microtrap by means of optical tweezers. The room-temperature trap setup and the cryostat are in a single vacuum chamber at a pressure of  $10^{-11}$  mbar. The optical tweezers are translated over 44 mm with an air-bearing translation stage outside the vacuum chamber.

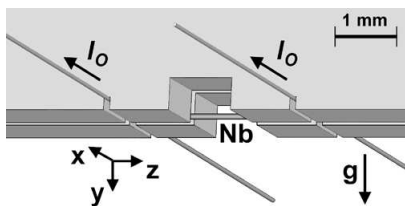


FIG. 2: Superconducting microtrap. The trap is generated below the Nb wire by applying a current  $I_{Nb}$  and a bias field  $\mathbf{B}_B$  in the positive  $x$ -direction. The Nb wire with circular cross section of diameter  $125 \mu\text{m}$  is clamped in a slit of a gold plated copper holder which is attached to the cryostat. It can be cooled to variable temperatures down to 4.2 K. A small cut in the copper holder gives free access to the Nb wire at the central part of the superconducting microtrap. A pair of kapton-insulated offset wires along the  $x$ -direction, just above the Nb wire, are used for the axial confinement of the trap. Gravity is along the  $y$ -direction.

is generated in the normal-conducting state. Transition to superconductivity is measured at  $T_c = 9.2$  K with a four-point probe.

In order to load atoms into the superconducting microtrap, we follow the experimental procedure as described below. Rubidium atoms ( $^{87}\text{Rb}$ ) from a dispenser are trapped and cooled in a six-beam MOT. After standard polarization gradient cooling and optical pumping to the  $|5S_{3/2}, F = 2, m_F = +2\rangle$  state the atoms are trapped in the quadrupole magnetic trap generated by the MOT coils. The atoms are then magnetically transferred via two transfer coils into an Ioffe-Pritchard-type trap which is generated by two smaller coils and a pair of wires parallel to the coil axis [1], as shown in Fig. 1. The strong confinement of this trap with radial and longitudinal oscillation frequencies of  $\omega_r = 2\pi \cdot 272 \text{ s}^{-1}$  and  $\omega_l = 2\pi \cdot 45 \text{ s}^{-1}$ , respectively, allows for efficient evaporative cooling. Radio-frequency evaporative cooling is applied for 13 s to obtain a thermal cloud of  $7 \cdot 10^5$  atoms at a temperature of  $2.5 \mu\text{K}$  [15].

After evaporative cooling the atoms are transferred into an optical dipole trap which is formed by focusing a 1064-nm laser with a 250-mm achromatic lens to a  $1/e^2$  beam waist radius of  $18 \mu\text{m}$ . The oscillation frequencies of the dipole trap are  $\omega_r = 2\pi \cdot 2100 \text{ s}^{-1}$  and  $\omega_l = 2\pi \cdot 30 \text{ s}^{-1}$ . The transfer is accomplished by ramping the laser light up to 500mW in 200 ms and then ramping down the magnetic field in 20 ms. Next, the atomic cloud is transported with the optical tweezers from the Ioffe-Pritchard-type trap over a distance of 44mm to the cold surface of the cryostat. For this purpose, the 250-mm lens is moved with an air-bearing linear translation stage (Aerotech, ABL 1000), which is placed next to the vacuum chamber (Fig. 1). The air-bearing stage is levitated with pressurized air and is driven by a brushless servo motor that guarantees minimal vibration and that has an accuracy of  $0.2 \mu\text{m}$ . Smooth transport is accomplished within 0.5 s using a sinusoidal acceleration profile with a maximum acceleration of  $1 \text{ m/s}^2$ .

The atoms are loaded from the optical tweezers into the superconducting microtrap at a distance of  $500 \mu\text{m}$  from the Nb wire. The loading is accomplished by ramping up the magnetic fields of the microtrap within 100 ms, and subsequently ramping down the laser power to zero in 0.5 s. The magnetic microtrap is generated by  $|\mathbf{B}_B| = 0.64 \text{ mT}$ ,  $I_{Nb} = 1.6 \text{ A}$  and  $I_0 = 0.01 \text{ A}$ . A homogeneous offset field  $|\mathbf{B}_0| = 0.1 \text{ mT}$  along the  $z$ -direction is additionally applied to reduce Majorana losses [1]. Both  $\mathbf{B}_B$  and  $\mathbf{B}_0$  are generated by Helmholtz coils outside the vacuum chamber. Trap frequencies are  $\omega_r = 2\pi \cdot 160 \text{ s}^{-1}$  and  $\omega_l = 2\pi \cdot 2 \text{ s}^{-1}$ . The microtrap is typically loaded with  $4 \cdot 10^5$  atoms at  $5 \mu\text{K}$ .

As the atoms are forced into the minimum of the magnetic trap, they can be used to probe the magnetic field profile near the superconducting wire, and in this way to assess the Meissner effect. The atoms are brought close to the Nb wire by reducing  $I_{Nb}$  while keeping  $\mathbf{B}_B$ ,  $I_0$  and  $\mathbf{B}_0$  constant. The positioning of the cloud is accom-

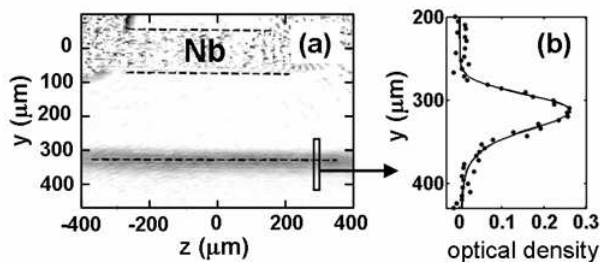


FIG. 3: (a) Absorption image of the atomic cloud at the central region of the magnetic trap. The dashed lines represent the longitudinal axis of the trap, and the Nb wire surface. (b) Optical density of one of the transverse sections of the atomic cloud. The best-fit curve  $\rho(y)$  is also plotted.

plished within 0.5 s, which is adiabatic with respect to the motion of atoms inside the trap. We measure the position  $y_0$  of the atom cloud with respect to the center of the superconducting Nb wire for different wire currents  $I_{Nb}$ . The data are derived from standard absorption images as shown in Fig. 3.

The atomic cloud in the microtrap is highly elongated due to the weak longitudinal confinement. In order to determine the longitudinal axis of the trap accurately, the absorption image of the cloud is divided into transverse sections. For every transverse section, the measured atom density is fitted by the theoretical atom density  $\rho(y)$  of a thermal cloud in a trapping potential  $U(y, x)$ , as seen in Fig.3(b). The asymmetry of the atom density profile is due to the decrease in magnetic gradient with increasing  $y$  and, to a lesser extent, due to gravity. These two effects are included in the potential  $U(y, x)$ . The maxima of  $\rho(y)$  of all transversal sections of the atomic cloud are fitted to a straight line, which is the longitudinal axis of the microtrap. The value of  $y_0$  is calculated as the distance between the longitudinal axis of the trap and that of the Nb wire.

Figure 4 (a) plots the trap position  $y_0$  as a function of  $I_{Nb}$ . Data are represented in logarithmic scale to give more visibility to the points that are closer to the wire. Measurements have been carried out for six different temperatures  $T$  of the Nb wire. The dependence of  $y_0$  on  $T$  is noticeable only at short distances from the wire, where the impact of the Meissner effect is stronger. For every temperature, the measured data are fitted by a theoretical curve that assumes that the superconducting Nb wire behaves like a diamagnetic cylinder of effective radius  $R$ . For every temperature, the best-fit curve is found by varying the effective radius  $R$ . Figure 4(b) represents the best-fit radius  $R$  versus  $T$ .

For comparison, the microtrap positions calculated for the normal-conducting state are represented as a dashed curve. It is a straight line, slightly distorted by gravity. Above  $T_c$  of Nb,  $\mathbf{B}_B$  penetrates the conductive wire and remains homogeneous, canceling the circular field of  $I_{Nb}$  at a distance from the wire center of  $y_{0,NC} = (\mu_0 I)/(2\pi B_B)$ . The magnetic-field gradient in

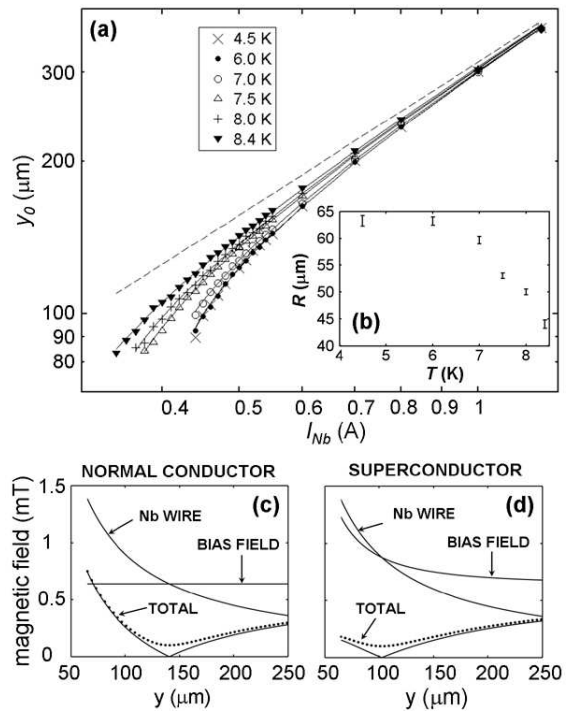


FIG. 4: (a) Distance between the trap center and the wire center as a function of the applied current  $I_{Nb}$  for six different temperatures.  $|\mathbf{B}_B| = 0.64$  mT,  $I_{Nb} = 1.6$  A and  $B_0 = 10^{-4}$  T. The normal-conducting case is represented as a dashed curve. The error bars, which result from the fitting procedure illustrated in Fig. 3, are smaller than the symbols and therefore not represented. (b) Best-fit radius as a function of the Nb wire temperature. The error bars represent the 95%-confidence interval. (c) and (d) Modulus of the magnetic-field profiles calculated for  $I_{Nb} = 0.45$ A for the normal-conducting and the superconducting cases, respectively. The comparison shows that the Meissner effect strongly distorts the bias field while leaving the field of  $I_{Nb}$  unchanged. This results in a lower trap depth and a shorter distance to the Nb wire. The realization of the microtrap requires that the bias field is opposite in direction to  $\mathbf{B}_{Nb}$ . The additional offset field  $B_0 = 10^{-4}$ T along the  $z$ -direction changes the magnetic profile from linear to parabolic (dotted curve).

the radial directions around  $y_{0,NC}$  is  $a_{NC} = B_B/y_{0,NC}$ . The gravitational sag is a small quantity that can be calculated as  $\Delta_{NC} = (gmB_0)/(g_F\mu_B m_F a_{NC}^2)$  [1].

Formulas describing the magnetic trap for the superconducting case are derived by approximating the Nb wire to a diamagnetic cylinder of effective radius  $R$ . Because of the axial symmetry, the magnetic field generated by  $I_{Nb}$  outside the superconducting wire is the same as in the normal case:  $B_{Nb} = (\mu_0 I_{Nb})/(2\pi y)$ . However, the bias field is strongly affected by the Meissner effect. The bias field on the  $y$ -axis becomes  $B_B(1+R^2/y^2) \mathbf{e}_x$  [16]. In the superconducting case, the bias field cancels the circular field of  $I_{Nb}$  at a distance from the wire center of

$$y_{0,SC} = \frac{\mu_0 I_{Nb}}{4\pi B_B} + \sqrt{\left(\frac{\mu_0 I_{Nb}}{4\pi B_B}\right)^2 - R^2}. \quad (1)$$

The magnetic-field gradient around  $y_{0,SC}$  is

$$a_{SC} = \frac{B_B}{y_{0,SC}} \left( 1 - \left( \frac{R}{y_{0,SC}} \right)^2 \right). \quad (2)$$

The gravitational sag  $\Delta_{SC} = (gmB_0)/(g_F\mu_B m_F a_{SC}^2)$  is always smaller than  $4\mu\text{m}$  and hardly affects the best-fit radius  $R$ . Even so, the effect of gravity on the trap position has been considered in the fitting procedure with the aim of reducing the error of the obtained best-fit  $R$ . The measured data are fitted by the function  $y_{0,SC} + \Delta_{SC}$ . For every temperature, the root-mean-square of the difference between the measured points and the best-fit curve is lower than  $2\mu\text{m}$ , which demonstrates that the magnetic field outside the Nb wire can be well described by formulas relying on a diamagnetic cylinder.

The way in which the Meissner effect changes the trap parameters is explained in Figs. 4 (c) and (d) by comparing the magnetic profiles in the superconducting and in the normal-conducting cases. The magnetic profile in the superconducting case is calculated assuming that the effective radius equals the real radius of the wire,  $R = 62.5\mu\text{m}$ . The Meissner effect shortens the distance between the trap and the wire, reduces the radial magnetic-field gradients and lowers the trap depth. The fact that the theoretical predictions for superconducting thin films reported in Ref. [13] follow a similar tendency suggests that this does not depend on the particular geometry of the superconductor.

The longitudinal confinement, which is very weak at the trap center because of the long distance between the offset wires, does not alter the trap parameters described in the above equations. It is also important to notice that the additional homogeneous offset field  $\mathbf{B}_0$  is not distorted by the Meissner effect because the longitudinal demagnetizing factor of a long cylinder quickly tends to zero as the strip length increases to infinity.

For temperatures lower than 6K, the best-fit radius  $R$  is very similar to the real radius of the wire. This is the expected value at such low temperatures, when the wire is in the pure Meissner state [17], i.e. when the magnetic flux penetrates the superconducting wire only to

the London depth, which is for Nb some tens of nanometers [18]. As the temperature is increased, the microtrap positions are shifted towards the positions expected for a normal-conducting wire. This is caused by an increase in the amount of magnetic flux penetrating the wire, which is manifested as a decrease of the effective radius  $R$ . The fact that the increase in temperature does not affect the points that are far from the wire demonstrates that the electric resistance remains zero, and so the applied current  $I_{Nb}$  flows entirely through the Nb wire. The experimental data reveal a smooth transition from the pure Meissner state to the normal state. For temperatures above 8.4 K, the atoms cannot be loaded into the microtrap because the critical current of the Nb wire drops below 1.6 A, which is the current  $I_{Nb}$  required to load the microtrap.

Another set of 160 measurements has been taken at  $T = 4.5$  K with different currents  $I_{Nb}$  in the range of 0.3 to 1.8 A and different bias fields in the range of 0.4 to 0.8 mT. By fitting the function  $y_{0,SC} + \Delta_{SC}$  to the overall data, we obtain an effective radius of  $(61.5 \pm 1.1)\mu\text{m}$ , which corroborates the presented results.

In conclusion, we demonstrated an experimental system that enables studies at the interface of cold atoms and superconductors. We measured the impact of the Meissner effect on the potential of a magnetic microtrap near a superconducting wire. The position of the atomic cloud reveals complete field exclusion from the superconducting wire for temperatures below 6 K. For higher temperatures, the microtrap parameters are sensitive to the temperature of the superconducting wire. Even though transition from the pure Meissner state to the normal state usually consists of complex processes involving vortex formation and penetration-depth increase [19], the trapping field outside the wire can be well described by simple formulas relying on a diamagnetic cylinder of effective, temperature-dependent radius  $R$ . The Meissner effect will have important implications for experiments with quantum gases near superconducting surfaces.

We thank Thomas Dahm for useful discussions. This work was supported by the DFG (SFB TRR 21) and by the BMBF (NanoFutur 03X5506).

- 
- [1] J. Fortágh, and C. Zimmermann, *Rev. Mod. Phys.* **79**, 235 (2007).
  - [2] C. Henkel, S. Pötting, M. Wilkens, *Applied Physics B* **69**, 379 (1999).
  - [3] M. P. A. Jones, C. J. Vale, D. Sahagun, B. V. Hall, and E. A. Hinds, *Phys. Rev. Lett.* **91**, 080401 (2003).
  - [4] D. M. Harber, J. M. McGuirk, J. M. Obrecht, and E. A. Cornell, *J. Low Temp. Phys.* **133**, 229 (2003).
  - [5] Y. J. Lin, I. Teper, C. Chin, and V. Vuletic, *Phys. Rev. Lett.* **92**, 050404 (2004).
  - [6] S. Scheel, P. K. Rekdal, P. L. Knight, and E. A. Hinds, *Phys. Rev. A* **72**, 042901 (2005).
  - [7] J. M. Obrecht, R. J. Wild, M. Antezza, L. P. Pitaevskii, S. Stringari, and E. A. Cornell, *Phys. Rev. Lett* **98**, 063201 (2007).
  - [8] U. Hohenester, A. Eiguren, S. Scheel, and E. A. Hinds, *Phys. Rev. A* **76**, 033618 (2007).
  - [9] P. Rabl, D. DeMille, J. M. Doyle, M. D. Lukin, R. J. Schoelkopf, and P. Zoller, *Phys. Rev. Lett.* **97**, 033003 (2006).
  - [10] A. S. Sorensen, C. H. van der Wal, L. I. Childress, and M. D. Lukin, *Phys. Rev. Lett.* **92**, 063601 (2004).
  - [11] C. Roux, A. Emmert, A. Lupascu, T. Nirrengarten, G. Nogues, M. Brune, J. -M. Raimond, and S. Haroche, *Europhysics Letters* **81**, 56004 (2008).
  - [12] T. Mukai, C. Hufnagel, A. Kasper, T. Meno, A. Tsukada,

- K. Semba, and F. Shimizu, Phys. Rev. Lett. **98**, 260407 (2007).
- [13] D. Cano, B. Kasch, H. Hattermann, D. Koelle, R. Kleiner, C. Zimmermann, and J. Fortágh, Phys. Rev. A **77**, 063408 (2008).
- [14] T. L. Gustavson, A. P. Chikkatur, A. E. Leanhardt, A. Görlitz, S. Gupta, D. E. Pritchard, and W. Ketterle, Phys. Rev. Lett. **88**, 020401 (2001).
- [15] Bose-Einstein condensation is reached with  $2 \cdot 10^5$  atoms by continuing evaporative cooling for another 5 s.
- [16] This formula can be deduced from the surface electric current  $\mathbf{K} = \mathbf{M} \times \mathbf{n}$  generated by the homogeneous magnetization  $\mathbf{M} = -2\mathbf{B}_B/\mu_0$  in the diamagnetic cylinder, where  $\mathbf{n}$  is the unit vector perpendicular to the cylinder surface. A similar deduction for the sphere can be found in J. D. Jackson *Classical electrodynamics* (John Wiley & Sons, Inc., 1967), Chap. 5.
- [17] F. London, *Superfluids* (Wiley, New York, 1950), Vol. I.
- [18] B. W. Maxfield and W. L. McLean, Phys. Rev. **139**, A1515 - A1522 (1965).
- [19] J. B. Ketterson, and S. N. Song, *Superconductivity* (Cambridge University Press, 1999).